

Journal of Materials Chemistry A

Accepted Manuscript



This is an *Accepted Manuscript*, which has been through the Royal Society of Chemistry peer review process and has been accepted for publication.

Accepted Manuscripts are published online shortly after acceptance, before technical editing, formatting and proof reading. Using this free service, authors can make their results available to the community, in citable form, before we publish the edited article. We will replace this *Accepted Manuscript* with the edited and formatted *Advance Article* as soon as it is available.

You can find more information about *Accepted Manuscripts* in the [Information for Authors](#).

Please note that technical editing may introduce minor changes to the text and/or graphics, which may alter content. The journal's standard [Terms & Conditions](#) and the [Ethical guidelines](#) still apply. In no event shall the Royal Society of Chemistry be held responsible for any errors or omissions in this *Accepted Manuscript* or any consequences arising from the use of any information it contains.

Preparation of ZnCo_2O_4 Nanoflowers on 3D Carbon Nanotube/Nitrogen-Doped Graphene Film and its Electrochemical Capacitance

Wenlong Bai , Hao Tong* , Zhenzhen Gao, Shihong Yue, Sichuan Xing, Shengyang Dong, Laifa Shen, Jianping He,

Xiaogang Zhang*, Yanyu Liang

Jiangsu Key Laboratory of Materials and Technology for Energy Conversion, College of Material Science and Engineering, Nanjing University of Aeronautics and Astronautics, Nanjing 210016, P. R. China.

Corresponding author: tongh@nuaa.edu.cn, azhangxg@163.com, azhangxg@nuaa.edu.cn

Abstract

Homogeneous ZnCo_2O_4 nanoflowers have been synthesized on a 3D layered structure of carbon nanotubes/nitrogen-doped graphene (NGN/CNTs) film by a hydrothermal process and subsequent calcination method. The ZnCo_2O_4 nanoflowers have an average diameter of 4 μm , and are composed by petals less than 100 nanometers. The as-synthetic ZnCo_2O_4 /NGN/CNTs film can be directly used as a flexible electrode with a high specific capacitance of 1802 F/g at 1 A/g and excellent cycling stability (almost 0% fade after 4000 sustaining charge/discharge at 10 A/g). These results suggest that the obtained electrode has a promising application prospect in flexible energy conversion/storage devices. In addition, a binder-free asymmetric supercapacitor has been synthesized with ZnCo_2O_4 /NGN/CNTs film as the positive electrode and NGN/CNTs film as the negative electrode. This demonstrates superior energy density (≈ 37.19 Wh/kg at 750 W/kg) and power density (≈ 14.992 kw/kg at 14.16 Wh/kg).

Keywords: ZnCo_2O_4 nanoflowers; carbon nanotubes/nitrogen-doped graphene film; flexible energy conversion/storage devices; asymmetric supercapacitor

Introduction

Nowadays, the energy conversion/storage devices have triggered abundant research for their potential applications in intelligent electronic equipment like tablet personal computer, smartwatch, smartband, intelligent vehicles and related products. But the energy conversion/storage devices face a major bottleneck to realize safe, light-weighted, wearable and flexible.¹⁻³ In recent years, supercapacitors with desirable performance of light-weight, long cycle life,

high power density, flexibility, non-toxic and fast charge/discharge rate,⁴⁻⁹ have been proposed as the next-generation wearable and flexible energy conversion/storage devices. Owing to rupture under slight tensile strain, transition metal oxides/sulfides with poor charge-discharge stability are unsatisfactory to be used directly into flexible electronic devices.¹⁰⁻¹⁷ Carbon materials like CNTs,¹⁸⁻²¹ Graphene (GN)^{7, 22} are appropriate to be used as flexible and stable electrode materials because of their excellent mechanical property and stable electrical performance. Among them, GN can be used as an outstanding flexible and stable electrode material with high-impact characteristics like large specific surface area, superb thermal conduction, great mechanical properties, controllable layer spacing and thickness, preferable theoretical electrical property and stable electric double layer structure.²³⁻²⁵ However, it is hard to achieve a theoretical specific surface area and specific capacitance because of serious overlap of GN sheets. So it is necessary and important to improve their electrochemical performance by expanding their specific surface area.²⁶ Up to now, Many works have been done by inserting CNTs between GN sheets to prevent stacking of GN.^{14, 18, 27, 28} For instance, Liu's group presented a novel method to fabricate self-supporting film through mixing few-walled CNTs and GN sheets to promote specific surface area and conductivity of GN, which is favorable for transport of ions and electrons, boosting rate capability and cyclic stability.²⁷ Lu *et al.* reported a flexible graphene/multiwalled carbon nanotubes (GN/MWCNTs) film.¹⁴ The electrochemical results demonstrate that the GN/MWCNTs film possesses a specific capacitance of 265 F/g at 0.1 A/g with a good rate capability (49 % capacity retention at 50 A/g), and displays an excellent specific capacitance retention of 97 % after 2000 continuous charge/discharge cycles.

Although prominent advantages have been obtained in electrode materials for this field, the relative unsatisfactory behaviors like low specific capacitance for carbon materials,¹⁴⁻¹⁶ may be still a biggest obstacle in actual application. Based on these facts, it is supposed to make further efforts to bring both the electronic double layer capacitor (EDLC) like GN, CNTs and pseudocapacitive like transition metal oxides/sulfides behavior

together. It has been already proven as an efficient method to satisfy the electrochemical performance after preparing a film for electrode materials, resulting in little electrical performance loss for its nanostructure and bulky specific surface area, which can provide abundant active sites for faraday reaction.¹⁷⁻²⁴

Among transition metal oxides, ternary metal oxides ZnCo_2O_4 with a spinel structure has a better specific capacitance and cycling life compared with Co_3O_4 or NiCo_2O_4 .²⁹⁻³³ Additionally, recent reports have demonstrated that ZnCo_2O_4 nanofibers, nanofleets and microspheres have achieved a high-performance electrochemical properties for supercapacitor.³⁴⁻³⁹ Wang *et al.* made ZnCo_2O_4 nanowires directly grow on nickel foam by a facile hydrothermal way and subsequent thermal treatment process. Electrochemical measurements show that the ZnCo_2O_4 /nickel foam electrode have a high specific capacitance (1625 F/g at 5 A/g), excellent rate capability (59 % capacitance retention at 80 A/g) and good cycling stability (94 % capacitance retention over 5000 charge–discharge cycles).³⁹ Wang *et al.* reported that hierarchical porous ZnCo_2O_4 microspheres have been successfully synthesized on nickel foam via a solvothermal method followed by an annealing process.⁴⁰ The ZnCo_2O_4 electrode shows a specific capacitance of 647.1 F/g at 1 A/g and 440.6 F/g at 10 A/g in 2 M KOH. After 2000 cycles, the capacity loss is 8.5%. However, all these methods need ZnCo_2O_4 to be loaded on nickel foam, which is too heavy as the current collector to be used in commercialization and also will dissolve into electrolyte in long-time charge–discharge cycles, resulting in its poor stability. Under this circumstance, it is necessary to use other support with light, good conductivity and long-life cycling stability to replace nickel foam to increase the high current cycling stability.

Here in, we use a cushy three-way procedures for the fabrication of hierarchical ZnCo_2O_4 nanoflowers on NGN/CNTs film via a hydrothermal synthesis method with doping nitrogen by ammonia reduction. NGN/CNTs film is obtained by filtration of the complex dispersion of graphene oxide (GO) and CNTs, which is conducive to increase wettability between electrode materials and electrolyte ions and may provide pseudocapacitance serving as

buffer to increase the cycling stability.^{41,42} Then $\text{ZnCo}_2\text{O}_4/\text{NGN}/\text{CNTs}$ precursor was obtained by a hydrothermal treatment on NGN/CNTs film. The subsequent measurements show that ZnCo_2O_4 nanoflowers load on NGN/CNTs film homogeneously. The hierarchical nanostructured electrode show a high specific capacitance of 1802 F/g at 1 A/g, promotional rate capability (63.74 % when the discharge current density arrange from 1 A/g to 25.5 A/g) and good cycling stability (almost 0 % fade after 4000 sustaining charge/discharge at 10 A/g). All of these may facilitate the progress of flexible electrochemical capacitance materials. Moreover, a high performance asymmetric supercapacitor is fabricated by using $\text{ZnCo}_2\text{O}_4/\text{NGN}/\text{CNTs}$ film as the positive electrode and NGN/CNTs film as the negative electrode. The cell voltage can reach 1.5V in an aqueous electrolyte, delivering high energy density (37.19 Wh/kg at 750W/kg) and high power density (\approx 14.992 kw/kg at 14.16 Wh/kg).

Experimental details

The schematic illustration of the representative synthetic method is presented in Fig.1. It clearly reveals that the entire process involves three steps: (1) the synthesis of NGN/CNTs film by vacuum filtration and subsequent doping nitrogen by ammonia reduction. (2) the ZnCo_2O_4 precursor loading on synthesis of NGN/CNTs film by hydrothermal treatment in a Teflon-lined stainless-steel Autoclave. (3) the synthesis of final product $\text{ZnCo}_2\text{O}_4/\text{NGN}/\text{CNTs}$ film after calcination.

Synthesis of NGN/CNTs film

Nitrogen-doped graphene (NGN) was synthesized from graphite flakes via an emerging method.⁴³ The homogeneous GO (100 ml, 0.5 mg/ml) was achieved by ultrasonication in an ultrasonic bath for half an hour. Then, the 1.5 g KMnO_4 was added slowly into the solution in order to activate GO. The mixture is stirred for 2 hours in a sealing condition. Successively, the mixture was reacted with HCl (30ml) and H_2O_2 (30ml) for 3 hours respectively to form homogeneous solution. The activated GO was subjected to dialysis to completely remove

remaining acids and salts. Acidifying multiwalled carbon nanotubes (95 % purity, 10-20 nm average diameter size, 100-160 g/m², ShenZhen Nanoport, LTD) was modified through concentrated sulfuric acid (15ml) for magnetic stirring 48 hours and was heated to 70 °C with a concentrated nitric acid for another 2 hours.²⁷ The mixture was further added 250 ml deionized water to prepare for next step (0.2 mg/ml). The resultant GO (33 ml) was under the ultrasonic for 30 minutes and was mixed with CNTs (8 ml) for another 1 hour. The resulting mixture was filtered by a vacuum filter with a 0.45 µm porous PTFE membrane to produce a GO/CNTs film. Subsequently, the GO/CNTs film was transferred to a Teflon-lined stainless steel autoclave with ammonium for doping nitrogen and reducing graphene, kept at 180 °C for 24 hours.

Synthesis of ZnCo₂O₄/NGN/CNTs film

In a typical process, Zn(NO₃)₂·6H₂O (1 mmol, 0.297 g), Co(NO₃)₂·6H₂O (2 mmol, 0.582 g), CO(NH₂)₂ (5 mmol, 0.300 g) and NH₄F (2 mmol, 0.074 g) were added into 45 ml distilled water and 30 ml alcohol under stirring to evolve a pink solution.⁴⁰ The prepared solution and NGN/CNTs film were moved into a Teflon-lined stainless-steel autoclave with a capacity of 100 ml, which were heating at 140 °C for 4 hours. After the reaction cooling to room temperature, the NGN/CNTs film coated with precursor was washed by distilled water, dried under vacuum at 30 °C for 24 hours, heated in a nitrogen atmosphere at 400 °C for 4 hours. In order to make a comparison of electrical performance with ZnCo₂O₄/NGN/CNTs film, we also synthesis ZnCo₂O₄/HGN/CNTs film under hydrazine hydrate reduction, NGN/CNTs film and ZnCo₂O₄/NGN film under the same conditions.

Material characterization

The microcosmic structure and morphology were investigated by transmission electron microscopy (TEM, JEOL JEM-2100), and field emission scanning electron microscopy (FE-SEM, Hitachi S-4800). The crystal structures of the samples were characterized by X-ray diffraction (XRD) (Bruker D8 advance) with Cu-K_α radiation. The X-ray photoelectron spectroscopy (XPS) analysis was performed on a Perkin-Elmer PHI 550 spectrometer with

Al-K α (1486.6 eV) as the X-ray source.

Electrochemical measurement

A three-electrode system were put into use to test the electrochemical activity of the synthetic samples. ZnCo₂O₄/NGN/CNTs film was used as a working electrode. A platinum plate electrode and saturated calomel electrode (SCE) served as the counter and reference electrode respectively. 6 M KOH was used as electrolyte.

Results and discussion

The micromorphology and architectural feature of the as-synthetic floriform ZnCo₂O₄ revealed by SEM and TEM. As shown in Fig. 2A and B, the nanoflowers grow on NGN/CNTs film uniformly. The diameter of the nanoflowers is approximately 2 μm with petal-like nanorods less than 100 nm thick and 1 μm long. These nanorods develop straightly and grow divergently from the core, so they can become self-support flower-like ZnCo₂O₄.

In order to observe the transformation from NGN/CNTs film to ZnCo₂O₄/NGN/CNTs film, we also made TEM for NGN/CNTs film in Fig. 3A and B. It can be seen that graphene sheets and nanotubes are integrated without bulky aggregates, which can be an ideal current collector for ZnCo₂O₄. The diameter of CNTs is nearly 10-20 nm, which is consistent with the size mentioned above. A 3D structure can be deduced from the interconnected nanotubes and crumpled graphene sheets which can increase the intrinsic electronic conductivity and rate capability. The nanoflowers ZnCo₂O₄ growing on the NGN/CNTs film demonstrate the ZnCo₂O₄ are tightly bound with the substrate in Fig. 3C and 3D.

A XRD pattern of the as-obtained ZnCo₂O₄ is shown in Fig. 2C. Except a few peaks from carbon material probably, other specific diffraction peaks in the pattern above almost accord with the spinel-like ZnCo₂O₄ (JCPDS card no.23-1390). The diffraction values in the Fig. 2C at 2 theta of 19.06°, 31.48°, 36.96°, 38.8°, 45.04°, 55.66°, 59.76°, 65.36° correspond to (111), (220), (311), (222), (400), (422), (511) and (440) crystal plane, separately. Moreover, the intensity of the sample was relatively small, which may derives from low diffraction intensities and

the influence of amorphous of NGN and CNTs. The chemical composition of NGN/CNTs film was characterized by XPS. The NGN/CNTs film include C1s, N1s, O1s from Fig. 4A. Fig. 4B shows deconvoluted N 1s XPS spectrum of as synthesized film. Five main peaks include pyridinic N at 398.3 eV, amino N at 399.2 eV, pyrrolic N at 400.1 eV, graphitic N at 401.4 eV and quaternary N at 403.7 eV. Based on the XPS survey spectra, the concentration of N is 9.8 %.

The capacitive property of as-obtained $\text{ZnCo}_2\text{O}_4/\text{NGN}/\text{CNTs}$ film electrode was explored by galvanostatic charge–discharge measurements and cyclic voltammetry (CV) in a 6 M KOH alkaline electrolyte. Fig. 5A illustrates the CV curves of the $\text{ZnCo}_2\text{O}_4/\text{NGN}/\text{CNTs}$ film electrode in a potential window between -0.15 to 0.6 V at scan rates from 2 to 100 mV/s. It is apparent that the presence of characteristic redox peaks confirms the pseudocapacitance feature. Compared with the CV curves of NGN/CNTs films in Fig. 5B, the CV curve of $\text{ZnCo}_2\text{O}_4/\text{NGN}/\text{CNTs}$ 3D nanoflowers has a larger area and current, indicating a better specific capacitance. The evident redox peaks are approximately owing to the reactions concern with Co-O/Co-O-OH, suggesting the excellent redox reversibility of the electrodes.⁴⁴

In order to accurately estimate the charge storage capacity, the electrochemical property of the as-synthetic electrode based on the charging and discharging at various current densities were also explored. The galvanostatic charge/discharge (GCD) measurements of $\text{ZnCo}_2\text{O}_4/\text{NGN}/\text{CNTs}$ film electrode have been performed in 6 M KOH. The Fig. 5C shows the GCD curves in a potential window of 0~0.5 V (vs. Hg/HgCl_2) at the current densities arranging between 1 and 25.5 A/g. All the charge/discharge curves are approximately symmetric with a slight bend, showing a typical pseudocapacitive characteristic. Especially there are voltage terrace at about 0.37 V and 0.3 V in the charge and discharge course respectively. According to the curves, the specific capacitance C_m can be calculated by the equation:

$$C_m = \frac{I \times \Delta t}{\Delta V}$$

Where Δt is the discharge time (s), I is the discharge current density (A/g), ΔV is the potential window (V), based on the equation mentioned, the obtained specific capacitances of the $\text{ZnCo}_2\text{O}_4/\text{NGN}/\text{CNTs}$ film electrodes are about 1802, 1530, 1400, 1320, 1200, 1150 F/g at current densities of 1, 2.5, 5, 10, 20, 25.5 A/g, respectively. It reveals that of the capacitance is still retained 63.74% when the discharge current density arrange from 1 A/g to 25.5 A/g. The total capacitance of $\text{ZnCo}_2\text{O}_4/\text{NGN}/\text{CNTs}$ film electrodes may be ascribed to three dominating contributions:(1) this newfangled structure supply plentiful active sites for faraday reaction and available electrolyte ions passageway for fast transportation. The electrochemical measurement results indicates that the electrical performance can be promoted by minishing the volume expansion in charge-discharging process and internal resistance due to this structure. (2) the gap between nanoflowers can improve the contact rate of electrolyte ions and NGN/CNTs film, which would boost rate capability. (3) The pyridine nitrogen could increase wettability between electrode materials and electrolyte ions and enhance electrical conductivity of graphene, resulting the increase of the specific capacitance.^{42,45}

The electrochemical impedance response (EIS) studies were explored in the frequency range between 100 kHz and 0.01 Hz in Fig. 5D-F. Fig. 4D shows the Nyquist of plots of the EIS spectra for $\text{ZnCo}_2\text{O}_4/\text{NGN}/\text{CNTs}$ film electrode and $\text{ZnCo}_2\text{O}_4/\text{NGN}$ film electrode, respectively. The internal resistances (R_s) showing subtle change at the high-frequency from intercept of the real axis suggest that the electron conductivity is almost the same. The charge transfer resistances (R_{ct}) estimated from the diameter of the semi-circle is decreasing obviously, implying that the ion diffusion and electrolyte penetration in the substrate materials are reduced. In addition, the EIS spectra of $\text{ZnCo}_2\text{O}_4/\text{NGN}/\text{CNTs}$ film electrode shows more vertical than $\text{ZnCo}_2\text{O}_4/\text{NGN}$ film electrode at the low frequency region, indicating electroactive material becomes more capacitive.⁴⁶ Fig. 5E shows the Nyquist of plots of $\text{ZnCo}_2\text{O}_4/\text{NGN}/\text{CNTs}$ film electrode before and after 4000 cycles. First, the internal resistance after 4000 cycles

grows rarely at the high-frequency intercept of the real axis, which indicates the electron conductivity of the film electrode fall insignificantly. Second, the diameter of the 1st and 4000th is similar, shows that the pathway for ion and electron transfer are keeping well. Furthermore, the EIS figure show tiny change and almost vertical line at the low frequency, indicating that the ion transport resistance keep so low after 4000 cycles and capacitance performance has improved though activation after 4000 cycles. And the slope of after 4000 cycles become a bit bigger than the original, illustrating the promotion of activation degree and utilization of ZnCo₂O₄ nanoflowers. The Nyquist of plots of GN under different reductant is showed in Fig. 5F. The internal resistances, charge transfer resistances and Warburg resistance (W) of ZnCo₂O₄/NGN/CNTs film electrode is better than the ZnCo₂O₄/HGN/CNTs film electrode, which is owing to the improvement of electrical conductivity by doping nitrogen.

Cycle stability is priority in actual application for battery industry. The Fig. 6A reveals the charging-discharging performance of ZnCo₂O₄/NGN/CNTs film electrode at a current density of 10 A/g in the three-electrode system. At the beginning 600 cycles, the specific capacitance rise up to 1360F/g, which is owing to the activation procedure of the ZnCo₂O₄. The specific capacitance conservation rate of the ZnCo₂O₄/NGN/CNTs film electrode is approximately 100% after 4000 charge-discharge cycles, which shows a superior property compared with the reported before.^{39,40} It is noteworthy that the natural growth in NGN/CNTs film as a electrical double-layer capacitor can prevent the collapse and decomposition of electrode materials under cycling charge-discharge and absorb a part of current as a buffer, which will enhance stability of oxide electrode .

The variation of C_m of NGN/CNTs film electrode, ZnCo₂O₄/NGN film electrode, ZnCo₂O₄/NGN/CNTs film electrode before charge-discharge cycles, ZnCo₂O₄/NGN/CNTs film electrodes after 4000th charge-discharge cycles (ZnCo₂O₄/NGN/CNTs film-4000th) and ZnCo₂O₄/HGN/CNTs film electrode with a steady increase in current density are displayed in Fig. 6B. As a whole, the ZnCo₂O₄/NGN/CNTs film-4000th has a better rate performance

than others. For instance, the C_m of NGN/CNTs film electrode can retain only 47.7 % when the current density increased from 2 A/g to 20 A/g. But the $ZnCo_2O_4/NGN/CNTs$ film-4000th can maintain 63.74 % of the value of 1 A/g and has a maximum of 1802 F/g after a loading of $ZnCo_2O_4$ nanoflowers, which derives from the synergetic combined contribution of the main redox pseudocapacitance of $ZnCo_2O_4$ and partly from the electric double-layer capacitance of NGN/CNTs in the composite.⁴⁷ The $ZnCo_2O_4/NGN$ film electrode can only keep 39.14% in the same condition for lacking of CNTs, demonstrating that CNTs can increase conductivity and enlarge specific surface area, resulting a better electrochemical performance. The influence after doping nitrating can be estimated between $ZnCo_2O_4/NGN/CNTs$ film-4000th and $ZnCo_2O_4/HGN/CNTs$ film electrode. Compared with ammonium reduction for $ZnCo_2O_4/HGN/CNTs$ film electrode, the C_m of $ZnCo_2O_4/HGN/CNTs$ film electrode with hydrazine hydrate reduction is obvious lower. Because nitrogen-Doping change the electron donor properties, leading to an improvement of the conductivity of carbon.⁴⁸ The C_m of $ZnCo_2O_4/NGN/CNTs$ film electrode will increase after charge-discharge cycles along with the improvement of activation degree and space utilization, which can be seen in Fig. 6B between $ZnCo_2O_4/NGN/CNTs$ film electrode before charge-discharge cycles and $ZnCo_2O_4/NGN/CNTs$ film-4000th. The commendable rate capability of $ZnCo_2O_4/HGN/CNTs$ film is keeping with the consequence from CV analysis. The preferable rate capability of $ZnCo_2O_4/NGN/CNTs$ film may be attributed to the subsequent two reasons. First of all, the homogeneous $ZnCo_2O_4$ nanoflowers growing on the surfaces of the NGN/CNTs films enable the electrolyte ion like OH^- approachable to $ZnCo_2O_4$ nanoflowers for faradaic reaction even at a high current density. Second, the pyridine nitrogen originating from doping nitrogen change the electron donor properties and then play an efficient role in conductivity of the materials in the electrochemical process, which can reduce the inner resistance of the film electrode.

In order to evaluate the $ZnCo_2O_4/NGN/CNTs$ film electrode for practical applications, an asymmetric supercapacitor (ASC) is fabricated by using $ZnCo_2O_4/NGN/CNTs$ film as the positive electrode and NGN/CNTs

film as the negative electrode in an aqueous electrolyte (6 M KOH) . Both those film electrode are pressed on Ni foam at a pressure of about 15 MPa. The mass ratio of $\text{ZnCo}_2\text{O}_4/\text{NGN}/\text{CNTs}$ to NGN/CNTs is controlled at 0.07 in the ASCs based on the charge balance at 1A/g for both electrodes. According to the Fig. 5B, the NGN/CNTs film shows a typical electric double-layer capacity characteristic in an KOH solution within the range -0.8~0 V. The $\text{ZnCo}_2\text{O}_4/\text{NGN}/\text{CNTs}$ film electrode display decent electrochemical performance within a potential window of -0.15~0.6 V from Fig. 5A. So the work potential of ASCs device is expected to 1.5 V. We performed a a range of CV texts with different potential windows to confirm the best operating potential from Fig. 7A. An obvious oxygen evolution appeared when the device is tested at a potential of 1.55 V. The operation voltage increases from 1.3 to 1.5 V with a increase from 107 to 119 F/g of the specific capacitance. The energy density of the ASCs is improved from 25.11 to 37.19 Wh/kg. So we choose 1.5 V to be the working voltage to further research the electrochemical performance. The CV curves of the ASCs have been detected between 0 and 1.5 V at scan rates arranging from 10 to 200 mV/s in Fig. 7B , which show nearly rectangular shapes without obvious redox peaks.

To further estimate the electrochemical performance of the as-fabricated ASCs device, galvanostatic charge/discharge (GCD) testing are performed with different current densities in a potential window of 0~1.5 V from Fig. 7C. The specific capacitance of $\text{ZnCo}_2\text{O}_4/\text{NGN}/\text{CNTs}/\text{NGN}/\text{CNTs}$ could reach 119 F/g at a current density of 0.5 A /g and still remain 54.46 F/g at a higher current density of 10 A/g. The triangular shape of charge/discharge curves are approximately symmetric also demonstrate the excellent capacitive behavior of the asymmetric supercapacitor in the whole potential region.

The energy and power densities of the asymmetric supercapacitor are calculated from discharge curves and plotted on the Ragone diagram shown in Fig. 7D. The maximum energy density of 37.19 Wh/kg (at a power density of 750 W/kg) and power density of 14992.14 W/kg (at a energy density of 14.16 Wh/kg) can be obtained at an operating voltage of 1.5 V. Which delivers higher energy density than $\text{MnO}_2\text{-graphene}/\text{CNT-graphene}$,⁴⁹

NiCo₂S₄//activated carbon,⁵⁰ NiCo₂S₄//RGO asymmetric supercapacitor.⁵¹

Conclusions

In summary, ZnCo₂O₄ nanoflowers have been loaded on NGN/CNTs film successfully through a facile hydrothermal way and subsequent thermal procedure. Benefitting from the layered structure and the favourable contact between the ZnCo₂O₄ nanoflowers and NGN/CNTs film, the film electrode can show a decent electrochemical characteristics. The as-obtained film electrode exhibits a high specific capacitance of 1802 F/g at 1 A/g and a great rate capability. More than that, the specific capacitance conservation rate of the ZnCo₂O₄/NGN/CNTs film electrode is approximately 100% after 4000 charge-discharge, which is the new flexible electrode materials for future energy storage equipment. Furthermore, we developed an asymmetric supercapacitors with ZnCo₂O₄/NGN/CNTs film as the positive electrode and NGN/CNTs film as the negative electrode. Which exhibits a superior energy density (≈ 37.19 Wh/kg at 750 W/kg) and power density (≈ 14.992 kw/kg at 14.16 Wh/kg). The present encouraging results opens up the possibility for manufacturing of high performance supercapacitors and other energy conversion/storage devices.

Acknowledgements

This work was supported by Priority Academic Program Development of Jiangsu Higher Education Institutions, the National Basic Research Program of China (973 Program) (No. 2014CB239701), National Natural Science Foundation of China (No. 21173120, 51372116, 51372115), Fundamental Research of Nanjing University of Aeronautics and Astronautics (NJ20150050).

References

1. N. S. Liu, W. Z. Ma, J. Y. Tao, X. H. Zhang, J. Su, L. Y. Li, C. X. Yang, Y. H. Gao, D. Golberg and Y. Bando, *Adv. Mater.*, 2013, **25**, 4925-4931.
2. X. H. Lu, Y. X. Zeng, M. H. Yu, T. Zhai, C. L. Liang, S. L. Xie, M. S. Balogun and Y. X. Tong, *Adv. Mater.*, 2014, **26**, 3148-3155.
3. M. F. El-Kady, V. Strong, S. Dubin, and R. B. Kaner, *Science*, 2012, **335**, 1326-1330.

4. J. R. Miller, P. Simon, *Science*, 2008, **321**, 651-652.
5. F. Wang, S. Xiao, Y. Hou, C. Hu, L. Liu and Y. Wu, *RSC Adv.*, 2013, **3**, 13059-13084.
6. G. Yu, X. Xie, L. Pan, Z. Bao and Y. Cui, *Nano Energy*, 2013, **2**, 213-234.
7. M. Yu, Y. Huang, C. Li, Y. Zeng, W. Wang, Y. Li, P. Fang, X. Lu and Y. Tong, *Adv. Funct. Mater.*, 2015, **25**, 324-330.
8. M. Yu, W. Qiu, F. Wang, T. Zhai, P. Fang, X. Lu and Y. Tong, *J. Mater. Chem. A*, 2015, **3**, 15792-15823.
9. M. Yu, W. Wang, C. Li, T. Zhai, X. Lu and Y. Tong, *NPG Asia Mater.*, 2014, **6**, e129.
10. A. Wang, H. Wang, S. Zhang, C. Mao, J. Song, H. Niu, B. Jin and Y. Tian, *Appl. Surf. Sci.*, 2013, **282**, 704-708.
11. H. Zhang, Y. Chen, W. Wang, G. Zhang, M. Zhuo, H. Zhang, T. Yang, Q. Li and T. Wang, *J. Mater. Chem. A*, 2013, **1**, 8593-8600.
12. G. Binitha, M. S. Soumya, A. A. Madhavan, P. Praveen, A. Balakrishnan, K. R. V. Subramanian, M. V. Reddy, S. V. Nair, A. S. Nair and N. Sivakumar, *J. Mater. Chem. A*, 2013, **1**, 11698-12704.
13. J. Zhang, J. Jiang and X. Zhao, *J. Phys. Chem. C*, 2011, **115**, 6448-6454.
14. X. Lu, H. Dou, B. Gao, C. Yuan, S. Yang, L. Hao, L. Shen, X. Zhang, *Electrochim. Acta*, 2011, **56**, 5115-5121.
15. C. Huang, N. Grobert, A. A. Watt, C. Johnston, A. Crossley, N. P. Young and P. S. Grant, *Carbon*, 2013, **61**, 525-536.
16. Y. Jang, J. Jo, Y. M. Choi, I. Kim, S. H. Lee, D. Kim and S. M. Yoon, *Electrochim. Acta*, 2013, **102**, 240-245.
17. I. K. Moon and K.-Y. Chun, *RSC Adv.*, 2015, **5**, 807-811.
18. L. Peng, Y. Feng, P. Lv, D. Lei, Y. Shen, Y. Li, and W. Feng, *J. Phys. Chem. C*, 2012, **116**, 4970-4978.
19. L. Hu, H. Wu and Y. Cui, *Appl. Phys. Lett.*, 2010, **96**, 183502.
20. J. Chen, A. Minett, I. Liu, Y. C. Lynam., P. Sherrell, C. Wang and G. G. Wallace, *Adv. Mater.*, 2008, **20**, 566-570.
21. H. Zhang, G. Cao, Z. Wang, Y. Yang and Z. Gu, *Carbon*, 2008, **46**, 822-824.
22. A. Yu, I. Roes, A. Davies and Z. Chen, *Appl. Phys. Lett.*, 2010, **96**, 253105.
23. A. A. Balandin, S. Ghosh, W. Bao, I. Calizo, D. Teweldebrhan, F. Miao and C. N. Lau, *Nano Lett.*, 2008, **8**, 902-907.
24. A. K. Geim and K. S. Novoselov, *Nat. Mater.*, 2007, **6**, 183-191..
25. Z. Li, B. Yang, S. Zhang and C. Zhao, *Appl. Surf. Sci.*, 2012, **258**, 3726-3731.
26. M. D. Stoller, S. J. Park, Y. W. Zhu, J. H. An and R. S. Ruoff, *Nano Lett.*, 2008, **8**, 3498-3502.
27. Y. Cheng, S. Lu, H. Zhang, C. V. Varanasi and J. Liu, *Nano Lett.*, 2012, **12**, 4206-4211.
28. M. Notarianni, J. Liu, F. Mirri, M. Pasquali and N. Motta, *Nanotechnol.*, 2014, **25**, 435405.
29. Y. Teng, L. X. Song, L. B. Wang and J. Xia, *J. Phys. Chem. C*, 2014, **118**, 4767-4773.
30. M. Liao, Y. Liu, Z. Hu and Q. Yu, *J. Alloys Compd.*, 2013, **562**, 106-110.
31. M. Yu, J. Chen, Y. Ma, J. Zhang, J. Liu, S. Li and J. An, *Appl. Surf. Sci.*, 2014, **314**, 1000-1006.
32. T. Y. Wei, C. H. Chen, H. C. Chien, S. Y. Lu and C. C. Hu, *Adv. Mater.*, 2010, **22**, 347-51.
33. X. Wang, W. S. Liu, X. Lu and P. S. Lee, *J. Mater. Chem.*, 2012, **22**, 23114-23119.
34. H. X. Chuo, H. Gao, Q. Yang, N. Zhang, W. B. Bu and X. T. Zhang, *J. Mater. Chem. A*, 2014, **2**, 20462-20469.
35. H. Wu, Z. Lou, H. Yang, and G. Shen, *Nanoscale*, 2015, **7**, 1921-6.
36. G. Zhou, J. Zhu, Y. Chen, L. Mei, X. Duan, G. Zhang, L. Chen, T. Wang and B. Lu, *Electrochim. Acta*, 2014, **123**, 450-455.
37. F. Bao, X. Wang, X. Zhao, Y. Ji Wang, Y. H. Zhang and X. Liu, *RSC Adv.*, 2014, **4**, 2393-2397.
38. R. Zhang, J. Liu, H. Guo and X. Tong, *Mater. Lett.*, 2014, **115**, 208-211.
39. S. Wang, J. Pu, Y. Tong, Y. Cheng, Y. Gao and Z. Wang, *J. Mater. Chem. A*, 2014, **2**, 5434.
40. Q. Wang, L. Zhu, L. Sun, Y. Liu and L. Jiao, *J. Mater. Chem. A*, 2015, **3**, 982-985.
41. H. F. Yen, Y. Y. Horng, M. S. Hu, W. H. Yang, J. R. Wen, A. Ganguly, Y. Tai, K. H. Chen and L. C. Chen, *Carbon*, 2015, **82**, 124-134.

42. G. Tian, L. Liu, Q. Meng and B. Cao, *J. Power Sources*, 2015, **274**, 851-861.
43. W. S. Hummers Jr, R. E. Offeman, *JACS*, 1958, **80**, 1339-1339.
44. B. Liu, Q. Wang, X. Wang, Q. Xiang, D. Chen and G. Shen, *ACS Appl. Mater. Interfaces*, 2013, **5**, 10011-10017.
45. L. F. Shen, J. Wang, G. Y. Xu, H. S. Li, H. Dou and X. G. Zhang, *Adv. Eng. Mater.*, 2014, **5**, Doi: 10. 1002/aenm. 201400977.
46. H. Chen, J. Jiang, Y. Zhao, L. Zhang, D. Guo and D. Xia, *J. Mater. Chem. A*, 2015, **3**, 428-437.
47. T. Y. Kim, H. W. Lee, M. Stoller, D. R. Dreyer, C. W. Bielawski, R. S. Ruoff and K. S. Suh, *ACS Nano*, 2011, **5**, 436-442.
48. L. Zhao, L. Z. Fan, M. Q. Zhou, H. Guan, S. Y. Qiao, M. Antonietti and M. M. Titirici, *Adv. Mater.*, 2010, **22**, 5202-5206.
49. Z. Y. Zhang, F. Xiao, L. Qian, J. Xiao, S. Wang and Y. Liu, *Adv. Energy. Mater.*, 2014, **4**, Doi: 10. 1002/aenm. 201400064.
50. Y. R. Zhu, Z. B. Wu, M. J. Jing, X. M. Yang, W. X. Song and X. B. Ji, *J. Power Sources.*, 2015, **273**, 584-590.
51. H. C. Chen, J. J. Jiang, L. Zhang, D. D. Xia, Y. D. Zhao, D. Q. Guo and H. Z. Wan, *J. Power Sources.*, 2014, **254**, 249-257.

Captions to figures

Fig.1 Schematic illustrations of the growth of ZnCo_2O_4 on NGN/CNTs film.

Fig.2 (A-B) SEM images and (C) XRD pattern of the $\text{ZnCo}_2\text{O}_4/\text{NGN}/\text{CNTs}$ film.

Fig.3 (A-B) TEM images of NGN/CNTs film and (C-D) TEM images of $\text{ZnCo}_2\text{O}_4/\text{NGN}/\text{CNTs}$ film .

Fig.4 (A) XPS spectra of NGN/CNTs film; (B) XPS spectra of N 1s.

Fig.5 (A) CV curves of the $\text{ZnCo}_2\text{O}_4/\text{NGN}/\text{CNTs}$ film electrode at various scan rates; (B) CV curves of the NGN/CNTs film electrode at various scan rates; (C) Charge and discharge curves of the $\text{ZnCo}_2\text{O}_4/\text{NGN}/\text{CNTs}$ film electrode at different current densities; (D) Nyquist plot of the $\text{ZnCo}_2\text{O}_4/\text{NGN}/\text{CNTs}$ film electrode and $\text{ZnCo}_2\text{O}_4/\text{NGN}$ film electrode; (E) Nyquist plot of the $\text{ZnCo}_2\text{O}_4/\text{NGN}/\text{CNTs}$ film electrode before and after 4000 charge and discharge cycles; (F) Nyquist plot of the $\text{ZnCo}_2\text{O}_4/\text{NGN}/\text{CNTs}/$ film electrode and $\text{ZnCo}_2\text{O}_4/\text{HGN}/\text{CNTs}/$ film electrode.

Fig.6 (A) cycling performance of the NGN/CNTs/ ZnCo_2O_4 film electrode at current densities of 5A g^{-1} . (B) specific capacitance as a function of the current of NGN/CNTs film electrode, $\text{ZnCo}_2\text{O}_4/\text{NGN}$ film electrode, $\text{ZnCo}_2\text{O}_4/\text{NGN}/\text{CNTs}$ film electrode, $\text{ZnCo}_2\text{O}_4/\text{NGN}/\text{CNTs}$ film -2000th and $\text{ZnCo}_2\text{O}_4/\text{HGN}/\text{CNTs}$ film electrode.

Fig.7 (A) CV curves of the ASCs at different potential window; (B) CV curves of the ASCs at various scan rates; (C) Charge and discharge curves of the ASCs at different current densities; (D) Ragone plots of the ASCs devices.

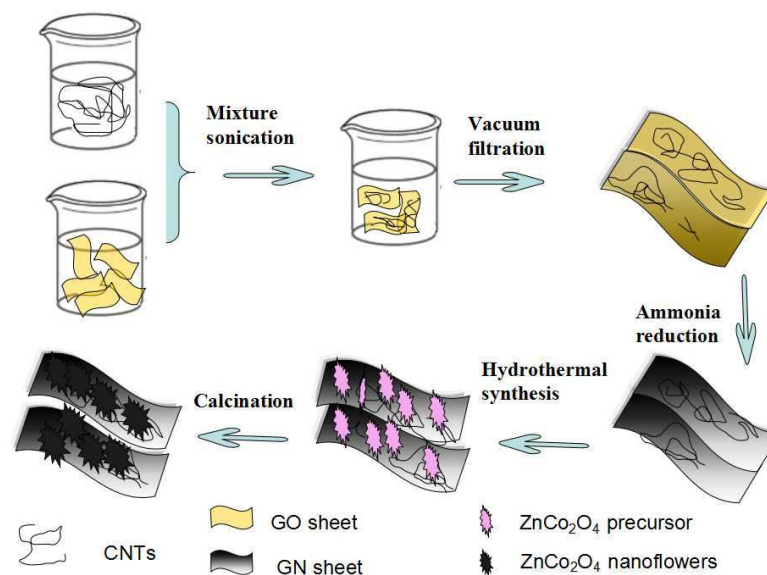


Fig. 1 Schematic illustrations of the growth of ZnCo₂O₄/NGN/CNTs film.

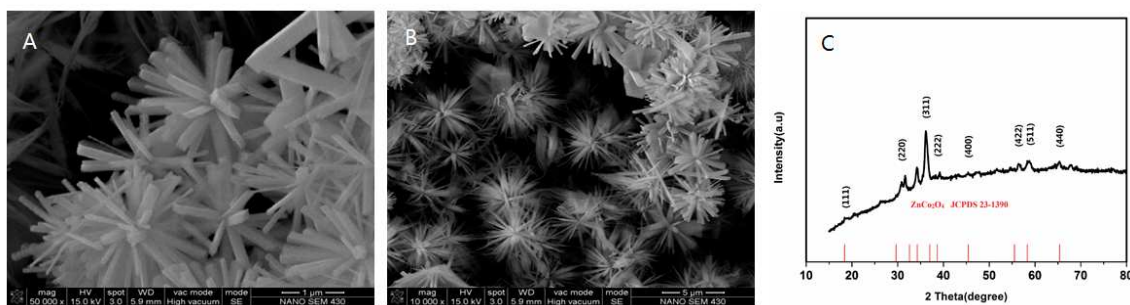


Fig.2 (A-B) SEM images and (C) XRD pattern of the ZnCo₂O₄/NGN/CNTs film

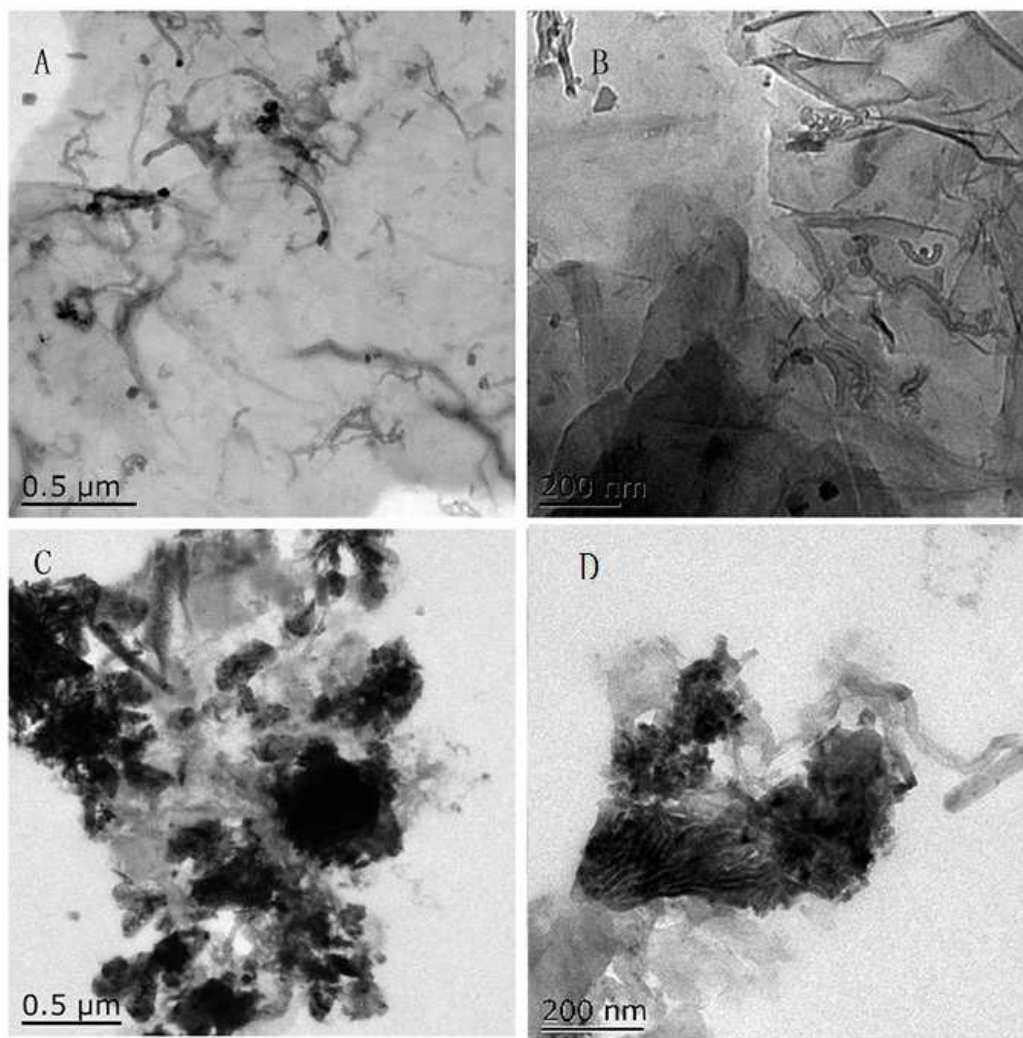


Fig.3 (A-B) TEM images of NGN/CNTs film and (C-D) TEM images of ZnCo₂O₄
/NGN/CNTs film

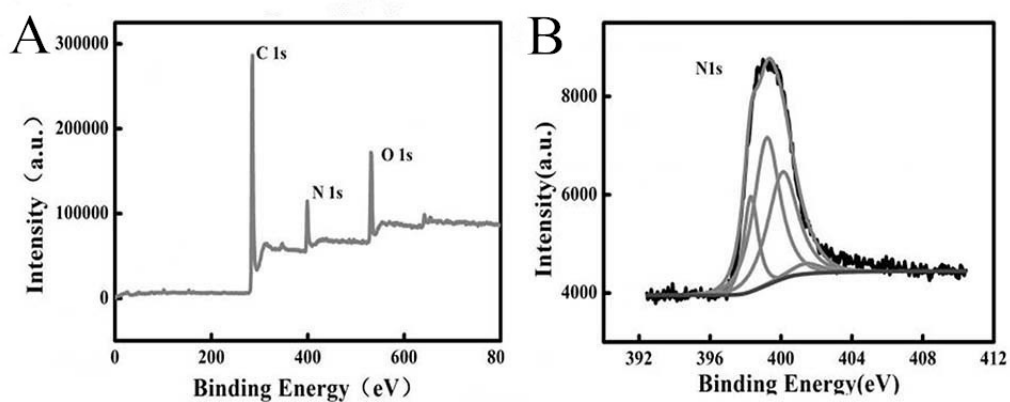


Fig.4 (A) XPS spectra of NGN/CNTs film; (B) XPS spectra of N 1s.

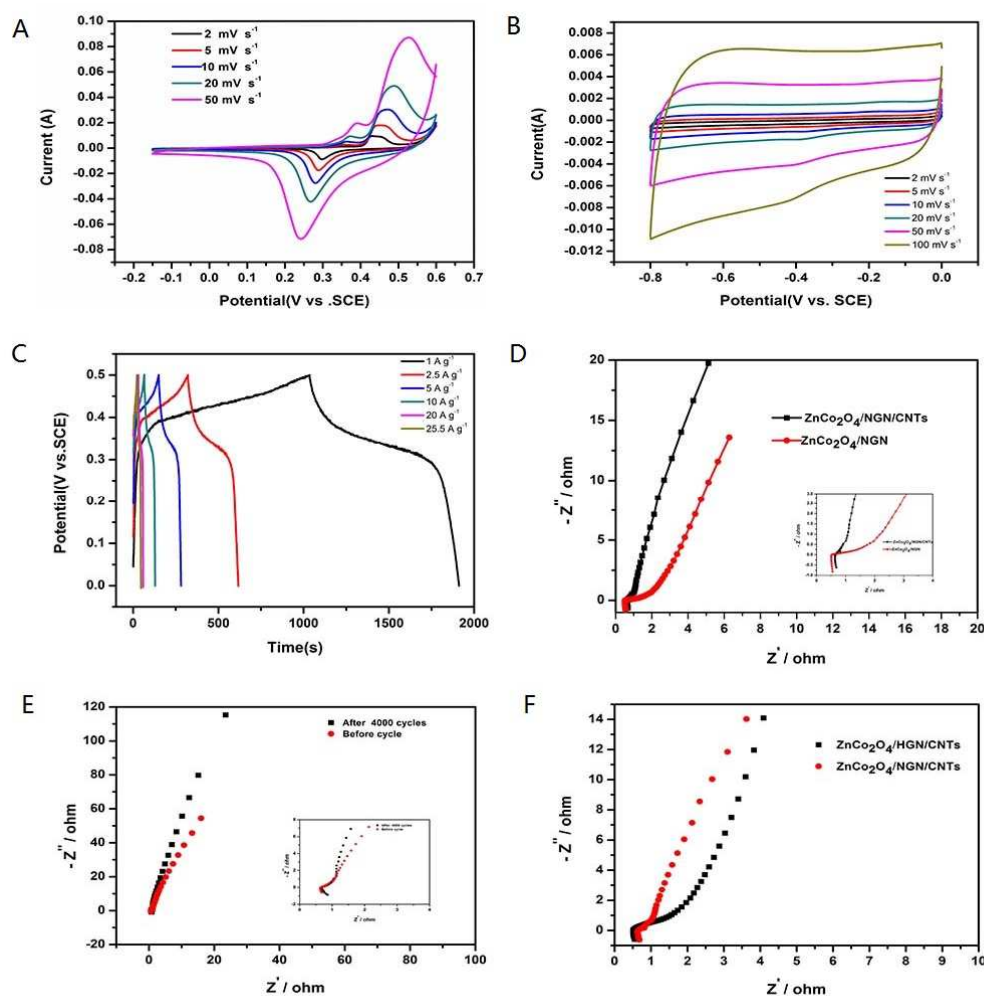


Fig.5 (A) CV curves of the NGN/CNTs/ ZnCo_2O_4 film electrode at various scan rates; (B) CV curves of the NGN/CNTs film electrode at various scan rates; (C) Charge and discharge curves of the NGN/CNTs/ ZnCo_2O_4 film electrode at different current densities; (D) Nyquist plot of the ZnCo_2O_4 /NGN/CNTs film electrode and ZnCo_2O_4 /NGN film electrode; (E) Nyquist plot of the ZnCo_2O_4 /NGN/CNTs film electrode before and after 4000 charge and discharge cycles; (F) Nyquist plot of the ZnCo_2O_4 /NGN/CNTs/ film electrode and ZnCo_2O_4 /HGN/CNTs/ film electrode.

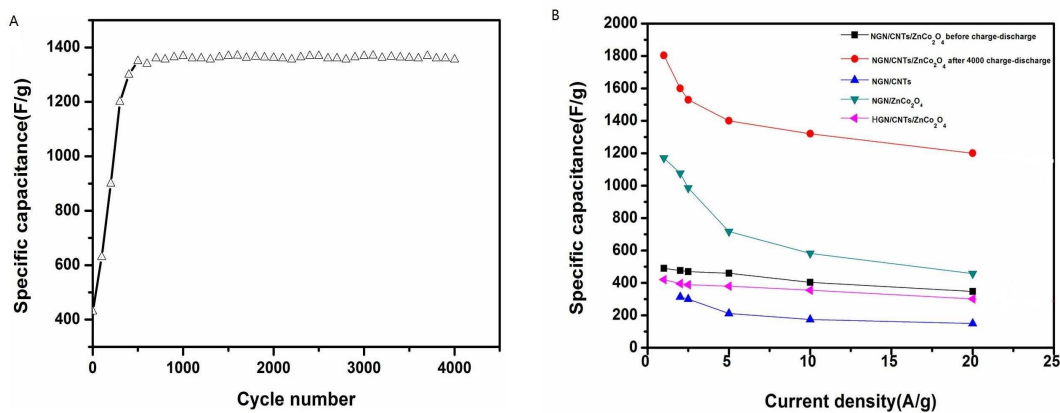


Fig. 6 (A) Cycling performance of the NGN/CNTs/ ZnCo_2O_4 film electrode at current densities of 5A g^{-1} . (B) Specific capacitance as a function of the current of NGN/CNTs film electrode, $\text{ZnCo}_2\text{O}_4/\text{NGN}$ film electrode, $\text{ZnCo}_2\text{O}_4/\text{NGN}/\text{CNTs}$ film electrode, $\text{ZnCo}_2\text{O}_4/\text{NGN}/\text{CNTs}$ film-4000th and $\text{ZnCo}_2\text{O}_4/\text{HGN}/\text{CNTs}$ film electrode.

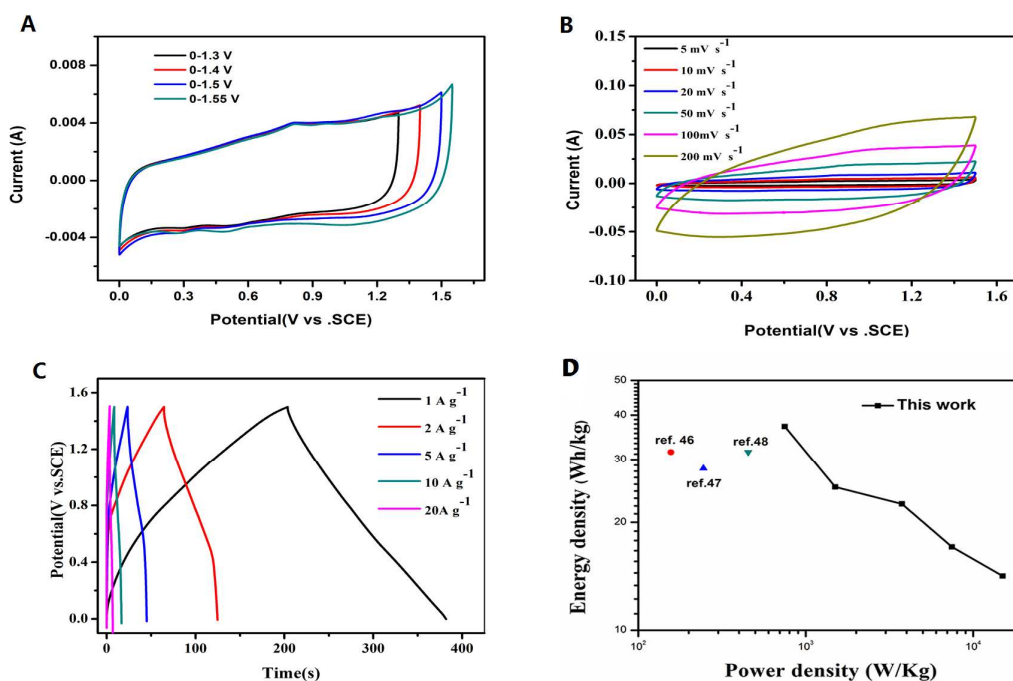


Fig. 7 (A) CV curves of the ASCs at different potential window; (B) CV curves of the ASCs at

various scan rates; (C) Charge and discharge curves of the ASCs at different current densities; (D)

Ragone plots of the ASCs devices.